Bloch-Nordsieck propagator at finite temperature

Jean-Paul Blaizot* and Edmond Iancu†
Service de Physique Théorique, CE-Saclay, 91191 Gif-sur-Yvette, France
(Received 30 June 1997)

We have shown recently that the resummation of soft photon contributions leads to a nonexponential decay of the fermion excitations in hot QED plasmas. The retarded propagator of a massless fermion was found to behave as $S_R(t\gg 1/gT)\sim\exp\{-\alpha Tt[\ln\omega_p t+C]\}$, where $\omega_p=gT/3$ is the plasma frequency, $\alpha=g^2/4\pi$, and C is a constant, independent of g, which was left undefined. This term is computed in this paper. In gauges with unphysical degrees of freedom, it is gauge-fixing independent provided an infrared regulator is introduced in the gauge sector. We also extend our analysis to hot QCD and express the quark and gluon propagators in the form of three-dimensional Euclidean functional integrals which may be evaluated on the lattice. [S0556-2821(97)00624-3]

PACS number(s): 11.10.Wx, 12.20.Ds, 52.60.+h

I. INTRODUCTION

The Bloch-Nordsieck (BN) approximation [1] offers an economical description of the nonperturbative interactions between charged particles and soft photons. At zero temperature, it provides the correct structure of the fermion propagator near the mass shell [2]. At finite temperature, the Bloch-Nordsieck approximation has been used, by Weldon, to verify the cancellation of the infrared divergences in the production rate for soft photons [3]. The remarkable structure of the ''hard thermal loops'' (HTL's) [4] emerges from similar kinematical approximations, as clearly emphasized in the kinetic derivation of the HTL's [5,6]. More recently, a similar approximation has been used in Refs. [7,8] to eliminate the infrared divergences in the computation of the fermion damping rate [9–12]. As shown in Ref. [8], this calculation requires the resummation of an infinite class of multiloop Feynman graphs of the type shown in Fig. 1. These are the same diagrams as those of the quenched approximation (i.e., all fermion loops are ignored), except for the fact that the photon lines include the hard thermal loop correction.

Throughout this work, we shall be mainly interested in the leading contribution of such diagrams to the propagator of a hard fermion ($p\gtrsim T$) near its mass shell ($p_0\sim p$). As shown in Ref. [8], this leading contribution can be estimated in the Bloch-Nordsieck approximation, that is, with the following simplified Feynman rules: (i) the fermion propagator

$$G_0(p-q)=\frac{1}{(p^0-q^0)-\mathbf{v}\cdot(\mathbf{p}-\mathbf{q})}; \tag{1.1}$$

(ii) the photon-fermion vertex $\Gamma^\mu=v^\mu$, and (iii) the HTL photon propagator $*_{D_{\mu\nu}(q)}$. Here, $p^\mu=(p_0,\mathbf{p})$ is the external hard momentum, with $p_0\simeq p$, $\mathbf{v}=\mathbf{p}/p$ is the corresponding velocity, $v^\mu\equiv(1,\mathbf{v})$, and $q^\mu=(q_0,\mathbf{q})$ is a linear combination of the soft momenta of the internal photons. The above Feynman rules govern the interactions between any kind of hard charged (or colored) particles, irrespective of their spin, and soft gauge fields, to leading order in an expansion in powers of the soft momenta [13] (see also Appendix C below for a discussion of the non-Abelian case). They lead to simplifications by ignoring those degrees of freedom—in this case, spin and negative-energy states—which play no dynamical role in the kinematical regime of interest.

The imaginary part of the fermion self-energy computed with these rules exhibits infrared divergences near the mass shell, to all orders in perturbation theory. For instance, in the one-loop approximation we have

$$\mathrm{Im}\,\Sigma_R^{(2)}(\omega\simeq p)\simeq-\alpha T\,\ln\frac{\omega_p}{|\omega-p|}, \tag{1.2}$$

where $\alpha\equiv g^2/4\pi$, $\omega_p=gT/3$ (the plasma frequency), and the approximate equality means that only the singular term has been preserved. For two or more photon loops, the mass-shell divergences are powerlike [8]. Such divergences prevent us from computing the mass-shell structure of the charged particles, and in particular from obtaining the fermion lifetime in perturbation theory.

Note, however, that no infrared divergences are encountered when the perturbation theory is carried out directly in the time representation: the inverse of the time acts then effectively as an infrared cutoff. For instance, the one-loop correction to the retarded propagator $S_R(t,\mathbf{p})$ at large times is given by

$$\delta S_R^{(2)}(t,\mathbf{p})\simeq-it\int_0^t dt'\,e^{ipt'}\Sigma_R^{(2)}(t',\mathbf{p}). \tag{1.3}$$

This expression is well defined although the limit $t\to\infty$ of the integral over t' [which is precisely the on-shell self-energy $\Sigma_R^{(2)}(\omega=p)$] does not exist. We actually have [8]

$$\Sigma_R^{(2)}(t,\mathbf{p})\simeq-i\alpha T\,\frac{e^{-ipt}}{t}\quad\text{for } t\gg\frac{1}{\omega_p}, \tag{1.4}$$

and, therefore,

$$\delta S_R^{(2)}(t,\mathbf{p})\simeq-\alpha Tt\int_{1/\omega_p}^t\frac{dt'}{t'}=-\alpha Tt\,\ln(\omega_p t). \tag{1.5}$$

*Also at CNRS.
†Also at CNRS.

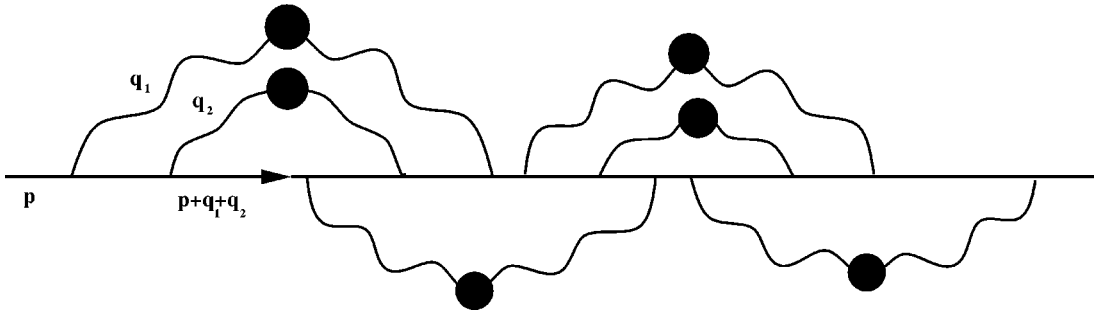

FIG. 1. A generic n-loop diagram (here, $n=6$) which is responsible for infrared divergences in perturbation theory. All the photon lines are soft and dressed by the hard thermal loop. The fermion line is hard and nearly on shell.

As shown in Refs. [7,8], this correction exponentiates in an all-order calculation:

$$S_R(t,\mathbf{p}) \propto \exp(-\alpha T t\, \ln \omega_p t) \quad \text{for } t \gg \frac{1}{\omega_p}. \tag{1.6}$$

Note, however, that the approximations used in Refs. [7, 8], and which lead to Eq. (1.6), are reliable only for computing the leading large-time behavior displayed in Eq. (1.6). (These approximations involve, aside from the Bloch-Nordsieck approximation, also a restriction to the static photon mode.) The subleading term—i.e., the constant term under the logarithm—could not be obtained in this way, and the issue of its gauge (in)dependence remained an entirely open problem.

In this paper, we improve the accuracy of our previous calculation by also including the nonstatic photon modes within the Bloch-Nordsieck calculation. This is sufficient to fix the term of order g^2T in the exponential (1.6). As we shall see, this term, which receives contributions from both the electric and the magnetic sectors, becomes gauge-fixing independent when an infrared regulator is introduced in the gauge sector. The final result, to be derived below, is

$$S_R(t \gg 1/\omega_p) \propto \exp\{-\alpha T t[\ln(\omega_p t) + 0.12652\ldots + \mathcal{O}(g)]\}. \tag{1.7}$$

This result applies to a massless fermion with momentum $p \sim T$ or larger. The extension to a massive ($m \gg T$) test particle is straightforward. The case of a soft fermion ($p \sim gT$), on the other hand, requires the full machinery of the HTL resummation [4], and will be not addressed here (see Ref. [8] for the leading order result in this case).

In order to derive Eq. (1.7), we shall use a finite-temperature extension of the Bloch-Nordsieck (BN) model, to be introduced in Sec. II. Formally, our construction is a straightforward generalization of the corresponding model at zero temperature, as described for example in Ref. [2]. However, unlike what happens at zero temperature, at finite temperature, the BN model cannot be solved in closed form (see also [8]). The technical difficulty comes from the thermal boundary conditions to be imposed on the BN propagator, and more specifically from the thermal occupation factors for the hard fermion. However, as it will be explained in Secs. III and IV, this problem can be overcome, within the desired accuracy, and this eventually yields the large-time behavior indicated in Eq. (1.7). The independence of this result with respect to the choice of the gauge is further analyzed in Sec. V. Finally, in Sec. VI, we consider an extension of the thermal BN model to QCD. Because of the mutual interactions of the soft gluons, the non-Abelian model cannot be solved analytically. Our main result here is an expression of the retarded propagator of a hard quark or gluon in the form of a functional integral over three-dimensional Euclidean gauge fields. This representation, which is reminiscent of the dimensional reduction sometimes performed in the computation of static thermal correlation functions [14,15], is well adapted to numerical calculations on a lattice.

II. THE BLOCH-NORDSIECK PROPAGATOR

As mentioned in the Introduction, we are interested in the large time decay of the propagator of a hard fermion moving through a QED plasma at very high temperature T: $T \gg m_e$, where m_e is the electron mass in the vacuum. This fermion can be either a thermal electron, with typical momentum $p \sim T$ and ultrarelativistic dispersion relation $E_p = p$ (we neglect the electron mass relative to T), or a (generally massive) test charged particle, with three-momentum $p \gtrsim T$ and dispersion relation $E_p = \sqrt{p^2+m^2}$. By test particle, we mean a particle which is distinguishable from the plasma particles, and is therefore not part of the thermal bath. The general formalism below will be developed for a thermal particle. We shall indicate later how one can derive from it the simpler case of the test particle. Also, we shall write the general formulas for a massless fermion. The corresponding formulas for a massive test particle will be presented only briefly.

We are eventually interested in the retarded propagator

$$iS_R(x-y) \equiv \theta(x_0-y_0)\langle\{\psi(x), \overline{\psi}(y)\}\rangle, \tag{2.1}$$

where the curly brackets denote the anticommutator of the fermion field operators, and the angular braces, the thermal expectation value. However, to calculate this propagator at finite temperature, it is convenient to consider first the time-ordered (or Feynman) propagator,

$$iS(x-y) \equiv \langle T\psi(x)\overline{\psi}(y)\rangle = \theta(x_0-y_0)S^>(x-y) - \theta(y_0-x_0)S^<(x-y), \tag{2.2}$$

and to observe that the two two-point functions

$$S^>(x-y) \equiv \langle \psi(x)\overline{\psi}(y)\rangle, \quad S^<(x-y) \equiv \langle \overline{\psi}(y)\psi(x)\rangle, \tag{2.3}$$

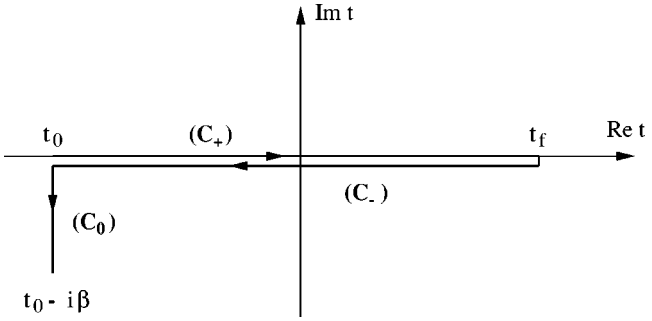

FIG. 2. Complex-time contour for the evaluation of the thermal expectation values: $C=C_+\cup C_-\cup C_0$. On C_+, t takes all the real values between t_0 to t_f (eventually, we let $t_f\to\infty$). On C_-, $t\to t-i0_+$, where t runs backward from t_f to t_0. Finally, on C_0, $t=t_0-i\tau$, with $0<\tau\leqslant\beta$.

are analytic functions of their time arguments. These functions can be first computed in the imaginary-time formalism [16], and then continued to the real-time axis. Then, the retarded propagator (2.1) can be obtained as

$$iS_R(x-y)=\theta(x_0-y_0)[S^>(x-y)+S^<(x-y)]. \quad (2.4)$$

This is a method that we have used in Ref. [8], and we shall use it again in Appendix A where we compute the propagator of a hard thermal fermion.

An alternative formalism, which permits a direct evaluation of real-time Green's functions, is based on the use of an oriented contour C in the complex time plane, as shown in Fig. 2 [16]. We define the contour-ordered propagator

$$iS(x-y)\equiv\langle T_C\psi(x)\overline{\psi(y)}\rangle=\theta_C(x_0,y_0)S^>(x-y)-\theta_C(y_0,x_0)S^<(x-y), \quad (2.5)$$

where the time variables x_0 and y_0 lie on C, and T_C and θ_C denote, respectively, the contour-ordering operator and the contour θ function. [If one gives a parametric representation of the path, $t=z(u)$, with u real and monotonically increasing, then path ordering corresponds to the ordering in u, and $\theta_C(t_1,t_2)=\theta(u_1-u_2)$.] The contour propagator (2.5) satisfies the Kubo-Martin-Schwinger (KMS) boundary condition [16]

$$S(t_0-y_0)=-S(t_0-y_0-i\beta). \quad (2.6)$$

(In this equation, and often below, we omit the spatial coordinates, for simplicity.) It can be given the following spectral representation [16]:

$$iS(x-y)=\int\frac{d^4p}{(2\pi)^4}\,e^{-ip\cdot(x-y)}\acute{\rho}(p)[\theta_C(x_0,y_0)-n(p_0)], \quad (2.7)$$

where $\acute{\rho}(p)$ is the fermion spectral density and $n(p_0)=1/[\exp(\beta p_0)+1]$. Note that, once the spectral density is known, the retarded propagator (2.1) can be obtained as

$$iS_R(x-y)=\theta(x_0-y_0)\int\frac{d^4p}{(2\pi)^4}\,e^{-ip\cdot(x-y)}\acute{\rho}(p). \quad (2.8)$$

In fact, in cases where we shall use the contour method below, the relation between S and S_R will be even simpler. Indeed, in these cases—that of a test particle, and that of a very energetic thermal particle, with $p\gg T$—the statistical factor $n(p_0)$ can simply be ignored, so that Eqs. (2.7) and (2.8) become identical for x_0 and y_0 real.

The large time behavior of the fermion propagator is governed by the interactions of the fermion with soft thermal photons. These can be analyzed in the BN approximation. The propagator has then the following functional integral representation [2] (see also Ref. [8]):

$$S(x-y)=Z^{-1}\int\mathcal{D}AG(x,y|A)e^{iS_C[A]}, \quad (2.9)$$

where $G(x,y|A)$ is the solution of the equation

$$i(v\cdot D_x)G(x,y|A)=\delta_C(x,y), \quad (2.10)$$

where $D_\mu=\partial_\mu+igA_\mu$, $v^\mu\equiv(1,\mathbf{v})$, $|\mathbf{v}|=1$, $\delta_C(x,y)$ is the contour delta function [16], and $S_C[A]$ is the effective action for soft photons in the hard thermal loop (HTL) approximation [4,6,16]

$$\begin{aligned}S_C[A]&=\int_C d^4x\left\{-\frac{1}{4}F_{\mu\nu}F^{\mu\nu}-\frac{1}{2\lambda}(\partial\cdot A)^2\right\}\\&\quad+\int_C d^4x\int_C d^4y\,\frac{1}{2}A^\mu(x)\Pi_{\mu\nu}(x,y)A^\nu(y)\\&\equiv\int_C d^4x\int_C d^4y\,\frac{1}{2}A^\mu(x)D^{-1}_{\mu\nu}(x-y)A^\nu(y).\end{aligned} \quad (2.11)$$

We have written this equation in the covariant gauge with parameter λ. The Coulomb gauge $\boldsymbol{\nabla}\cdot\mathbf{A}=0$ will also be used in what follows. $\Pi_{\mu\nu}$ is the photon polarization tensor in the HTL approximation [17,4].

The gauge fields to be integrated over in Eq. (2.9) satisfy the periodicity condition $A_\mu(t_0,\mathbf{x})=A_\mu(t_0-i\beta,\mathbf{x})$. Correspondingly, the photon contour propagator satisfies

$$D_{\mu\nu}(t_0-y_0)=D_{\mu\nu}(t_0-y_0-i\beta), \quad (2.12)$$

and can be given the following spectral representation:

$$D_{\mu\nu}(x-y)=-i\int\frac{d^4q}{(2\pi)^4}\,e^{-iq\cdot(x-y)}\rho_{\mu\nu}(q)\times[\theta_C(x_0,y_0)+N(q_0)], \quad (2.13)$$

where $\rho_{\mu\nu}(q)$ is the photon spectral density in the HTL approximation [18] (we follow here the notations in Ref. [8]), and $N(q_0)=1/[\exp(\beta q_0)-1]$ is the Bose-Einstein statistical factor.

Equation (2.10) defines the BN propagator of a charged particle in a classical background field $A_\mu(x)$. The vector $\mathbf{v}$ in this equation is to be identified with the particle velocity. Then, the Feynman rules generated by the functional integral (2.9) coincide with those given in the introduction. Since, in the BN model, $\mathbf{v}$ is a fixed parameter, the underlying physical approximation is the lack of fermion recoil. This approxi-

mation is justified when the momentum transfer from the background field is small, at most of order $\sim gT$. (The energy-momentum scale gT is set by the polarization tensor $\Pi_{\mu\nu}$; see Sec. III below.)

In order to satisfy the KMS condition (2.6), the BN equation (2.10) has to be solved for antiperiodic boundary conditions

$$G(t_0,y_0|A)=-G(t_0-i\beta,y_0|A), \tag{2.14}$$

and similarly for y_0. These conditions complicate the resolution of the thermal BN model in general. There is a simple case, however, where this complication is absent, namely, the case of a test particle. For this case, the thermal BN model can be exactly solved, as we discuss now.

A. The test particle

The propagator of a test particle has only one analytic component, namely, $S^>(x-y)$; $S^<$ vanishes since the thermal bath acts as the vacuum for the field operators of the test particle. Therefore [cf. Eqs. (2.1)–(2.4)], $S(x-y)=S_R(x-y)=-i\theta(x_0-y_0)S^>(x-y)$ and the KMS conditions (2.6) do not apply. In the BN approximation, $S(x,y)$ is still given by Eq. (2.9), but now $G(x,y|A)$ obeys retarded conditions in real time, and not the conditions (2.14). The solution to Eq. (2.10) is then obtained in closed form [2] (see also Ref. [8]):

$$\begin{aligned}G_R(x,y|A)&=-i\theta(x^0-y^0)\,\delta^{(3)}(\mathbf{x}-\mathbf{y}-\mathbf{v}(x^0-y^0))U(x,y)\\&=-i\int_0^\infty dt\,\delta^{(4)}(x-y-vt)U(x,x-vt),\end{aligned} \tag{2.15}$$

where the time variables x_0 and y_0 are real. The three-dimensional δ function describes straightline propagation with velocity v. The background gauge field only contributes a phase factor:

$$U(x,x-vt)\equiv\exp\left\{-ig\int_0^t ds\; v\cdot A(x-v(t-s))\right\}. \tag{2.16}$$

In momentum space, the free ($A_\mu=0$) retarded propagator reads

$$G_R^0(\omega,\mathbf{p})=\frac{1}{\omega-\mathbf{v}\cdot\mathbf{p}+i\eta}, \tag{2.17}$$

corresponding to the following free spectral density:

$$\rho_0(\omega,\mathbf{p})\equiv-2\,\mathrm{Im}G_R^0(\omega,\mathbf{p})=2\pi\delta(\omega-\mathbf{v}\cdot\mathbf{p}). \tag{2.18}$$

According to these equations, the fermion mass shell in the BN model corresponds to $\omega=E_p\equiv\mathbf{v}\cdot\mathbf{p}$. Since v is to be identified with the velocity $\mathbf{p}/p$ of the massless fermion, the free mass shell is at $\omega=p$, as it should.

In order to perform the functional integration (2.9), we first rewrite the parallel transporter (2.16) as

$$U(x,x-vt)=\exp\left\{-i\int d^4z\,j_\mu(z)A^\mu(z)\right\},$$

$$j_\mu(z)\equiv gv_\mu\int_0^t ds\,\delta^{(4)}(z-x+v(t-s)). \tag{2.19}$$

Then, a straightforward calculation yields

$$S_R(t,\mathbf{p})=-i\theta(t)e^{-it(\mathbf{v}\cdot\mathbf{p})}\widetilde{\Delta}(t), \tag{2.20}$$

with

$$\widetilde{\Delta}(t)=\exp\left\{-\frac{i}{2}\int_{C_+}d^4x\int_{C_+}d^4y\;j^\mu(x)D_{\mu\nu}(x-y)j^\nu(y)\right\}, \tag{2.21}$$

where the time integrals run on C_+ only, in accordance with Eq. (2.19).

By using Eqs. (2.19) and (2.13), and after a simple calculation, we can rewrite $\widetilde{\Delta}(t)$ in Eq. (2.21) as

$$\widetilde{\Delta}(t)=\exp\left\{-\frac{g^2}{2}\int\frac{d^4q}{(2\pi)^4}\int_0^t ds_1\int_0^t ds_2 e^{-i(q\cdot v)(s_1-s_2)}\widetilde{\rho}(q)\times[\theta(s_1-s_2)+N(q_0)]\right\}, \tag{2.22}$$

with $\widetilde{\rho}(q)\equiv v^\mu\rho_{\mu\nu}(q)v^\nu$. Note that Eq. (2.22) could have been obtained from the corresponding expression in the vacuum (see Ref. [2]) by simply replacing in the latter the bare photon propagator by the corresponding thermal propagator for a soft photon. Conversely, the zero-temperature *BN* propagator can be obtained from Eq. (2.22) by substituting $N(q_0)\to-\theta(-q_0)$ and replacing $\rho_{\mu\nu}$ with the free photon spectral density.

After performing the s_1 and s_2 integrations, and also using the parity property $\widetilde{\rho}(-q)=-\widetilde{\rho}(q)$, we finally cast Eq. (2.22) into the form

$$\widetilde{\Delta}(t)=\exp\{it\Phi(t)\}\Delta(t), \tag{2.23}$$

where

$$\Phi(t)\equiv g^2\int\frac{d^4q}{(2\pi)^4}\frac{\widetilde{\rho}(q)}{2(v\cdot q)}\left[1-\frac{\sin t(v\cdot q)}{t(v\cdot q)}\right], \tag{2.24}$$

and

$$\Delta(t)\equiv\exp\left\{-g^2\int\frac{d^4q}{(2\pi)^4}\,\widetilde{\rho}(q)N(q_0)\,\frac{1-\cos t(v\cdot q)}{(v\cdot q)^2}\right\}. \tag{2.25}$$

In the derivation of the above formulas, Eqs. (2.22)–(2.25), there was no explicit restriction on the photon momenta q^μ. Since the *BN* model can only be trusted for soft photons, we need to verify that the large time behavior of the fermion propagator, as given by Eqs. (2.20)–(2.25), is indeed controlled by soft momenta, $q\ll T$.

In fact, the momentum integrals in Eqs. (2.24)–(2.25) contain ultraviolet divergences coming from their zero-temperature contributions. There is a linear UV divergence in $\Phi(t)$, and a logarithmic divergence in $\Delta(t)$. These diver-

gences can be absorbed respectively, by mass and field-strength renormalizations [2]. However, the finite part of the phase $\Phi(t)$ remains dominated by hard momenta contributions, and therefore is not consistently determined by the present approximation. Since $\Phi(t)$ does not enter the calculation of the lifetime, we shall ignore it in what follows.

The damping effects are entirely described by the function $\Delta(t)$, Eq. (2.25), which extends our previous result [7,8] by including the effects of the nonstatic ($q_0 \neq 0$) electric and magnetic field fluctuations. At $T=0$, $\Delta_{T=0} \propto \exp(-g^2 \ln \Lambda t)$, where Λ is the upper momentum cutoff [2]. After UV renormalization, the cutoff Λ is replaced by the physical electron mass, thus yielding

$$|S(t)| \sim (mt)^{(3-\lambda)(\alpha/2\pi)}, \tag{2.26}$$

in the covariant gauge with gauge-fixing parameter λ [see Eq. (4.11)]. Such a gauge-dependent, polynomial dependence on time merely reflects the renormalization of the wave function of the fermion due to its coupling to soft virtual photons. This is not to be interpreted as a damping phenomenon. The mechanism which takes place at high temperature and which eventually gives rise to the damping of the test particle excitation is the exchange of soft photons between the test fermion and the thermal charged particles. We shall verify in Sec. III that, for sufficiently large times $t \gg 1/gT$, such a collision involves dominantly soft photon momenta $q \lesssim gT$.

For a fixed large time t, the function

$$f(t, v\cdot q) \equiv \frac{1-\cos t(v\cdot q)}{(v\cdot q)^2}, \tag{2.27}$$

in Eq. (2.25) is strongly peaked around $v\cdot q \equiv q_0 - \mathbf{v}\cdot\mathbf{q} = 0$, with a width $\sim 1/t$. In the limit $t\to\infty$, $f(t, v\cdot q) \to \pi t \delta(v\cdot q)$. In the absence of infrared complications, we could use this limit to obtain the large time behavior of $\Delta(t)$. This procedure would then yield $\Delta(t\to\infty) \sim e^{-\gamma t}$, with

$$\gamma \equiv \pi g^2 \int \frac{d^4q}{(2\pi)^4}\, \tilde{\rho}(q) N(q_0)\, \delta(v\cdot q). \tag{2.28}$$

We recognize in Eq. (2.28) the one-loop damping rate $\gamma = -\mathrm{Im}\Sigma^{(2)}(\omega = p)$ [11,12], which we know, however, to be infrared divergent [cf. Eq. (1.2)]. Thus, in studying the large-time behavior of Eq. (2.25), one should keep the time finite when performing the momentum integral. As already mentioned after Eq. (1.3), the inverse time plays the role of an infrared cutoff. This will become explicit in Sec. III below.

Equations (2.20)–(2.25) generalize trivially to a test particle with mass m. The mass shell is shifted to $E_p \equiv \mathbf{v}\cdot\mathbf{p} + m(1-\mathbf{v}^2)^{1/2}$ (which, since $\mathbf{v} = \mathbf{p}/E_p$, corresponds indeed to $E_p = \sqrt{p^2+m^2}$), and the retarded propagator has the form (2.20):

$$|S_R(t,\mathbf{p})| = \theta(t)\Delta_v(t), \tag{2.29}$$

where $\Delta_v(t)$ is the function (2.25) with, however, $|v| < 1$.

B. The thermal fermion

The case of a thermal electron with momentum $p \sim T$ is physically more interesting, since this is a typical quasiparticle of the plasma. Technically, however, this is more involved, since the KMS boundary conditions (2.14) must be taken into account.

To appreciate the difficulty, consider the free contour propagator, as obtained by replacing $\acute{\rho}(p)$ with $\acute{\rho}_0(p) = 2\pi\delta(\omega - \mathbf{v}\cdot\mathbf{p})$ in Eq. (2.7):

$$G_0(t-t',\mathbf{p}) = -ie^{-i(\mathbf{v}\cdot\mathbf{p})(t-t')}[\,\theta_C(t,t')(1-n_p) - \theta_C(t',t)n_p], \tag{2.30}$$

where $n_p \equiv n(\mathbf{v}\cdot\mathbf{p})$. By using this propagator, we can solve the BN equation (2.10) as a series in powers of gA_μ. To this aim, one can first transform Eq. (2.10) into an integral equation:

$$G(x,y|A) = G_0(x-y) + g\int_C d^4z\; G_0(x-z)v\cdot A(z) G(z,y|A). \tag{2.31}$$

Then, by iteratively solving this equation, one generates the perturbation series for $G(x,y|A)$. However, in contrast to what happens for the retarded propagator (2.15), the resulting series for the contour propagator $G(x,y|A)$ does not exponentiate [8]. The exponentiation of the perturbative series for $G_R(x,y|A)$ is related to the fact that the retarded free propagator,

$$G_R^0(t,\mathbf{p}) = -i\,\theta(t)e^{-i(\mathbf{v}\cdot\mathbf{p})t}, \tag{2.32}$$

satisfies the simple multiplication law $G_R^0(t,\mathbf{p}_1)G_R^0(t,\mathbf{p}_2) = -G_R^0(t,\mathbf{p}_1+\mathbf{p}_2)$. The contour propagator $G_0(t,\mathbf{p})$ does not enjoy this property, because of the presence of the statistical factors in Eq. (2.30).

This argument suggests that the contour BN propagator may exponentiate whenever the fermion occupation numbers play no dynamical role. This is what happened for the test particle in the previous subsection, and, more generally, this will also happen for a thermalized fermion with very high momentum $p \gg T$ whose thermal occupation number is exponentially small: $n(p) \simeq e^{-\beta p} \ll 1$. In fact, when $n_p \to 0$, the free contour propagator (2.30) reduces to the retarded function (2.32) (for real time variables). It is then easy to verify that the previous solution of the BN model, as given by Eqs. (2.20)–(2.25), also applies to such a very energetic thermal particle, up to corrections which are exponentially small when $p \gg T$. In particular, the case of the test particle is formally recovered as the limit $p/T \to \infty$.

What is less obvious is that the same solution holds also for a typical thermal fermion, with momentum $p \sim T$. More precisely, as will be verified in Appendix A, the thermal fermion propagator decays according to the same law as above, that is,

$$|S_R(t,\mathbf{p})| \propto \Delta(t) \tag{2.33}$$

[with $\Delta(t)$ as defined in Eq. (2.25)], up to corrections of order $q/T \lesssim g$. Physically, this reflects the fact (which has been already mentioned at several places, and will be verified in the next section) that the fermion decay at large times, $t \gg 1/gT$, is determined by its interactions with soft photons, with momenta $q \lesssim gT$. Such interactions do not significantly change the electron momentum, so that the associated thermal occupation factors play no dynamical role.

III. LARGE TIME BEHAVIOR

We are now in a position to study the large-time behavior of the fermion propagator, as described by the function $\Delta(t)$, Eq. (2.25). We shall verify below that the relevant energy scale is hidden in the photon spectral density $\rho_{\mu\nu}(q)$, and is of the order gT. Therefore, ''large times'' means times larger than $1/gT$.

For the computation below, we shall use the photon spectral density in the Coulomb gauge

$$\widetilde{\rho}(q_0,\mathbf{q}) = \rho_l(q_0,q) + [1-(\mathbf{v}\cdot\hat{\mathbf{q}})^2]\rho_t(q_0,q). \tag{3.1}$$

(The issue of the gauge dependence will be addressed in the next section.) The two pieces $\rho_l(q_0,q)$ and $\rho_t(q_0,q)$ of the spectral density correspond, respectively, to longitudinal and transverse photons, which are renormalized differently by plasma effects [6,16]. They have the following structure (with $s=l$ or t):

$$\rho_s(q_0,q) = 2\pi\epsilon(q_0) z_s(q)\,\delta[q_0^2-\omega_s^2(q)] + \beta_s(q_0,q)\,\theta(q^2-q_0^2), \tag{3.2}$$

and involve δ functions associated to plasma waves at time-like momenta ($q_0^2=\omega_s^2(q)>q^2$), and smooth contributions β_l and β_t at $q_0^2<q^2$ arising from Landau damping. For given q_0 and q, the energy-momentum scale in Eq. (3.2) is set by the plasma frequency $\omega_p \equiv gT/3$, for both the on-shell and the off-shell spectral densities (see [18,6,16] for more details).

For generic times, both pieces in Eq. (3.2) contribute to Eq. (2.25).

(i) That involving $\delta[q_0^2-\omega_s^2(q)]$ describes the emission or the absorption of an on-shell plasmon. By kinematics, this is only possible if the fermion is sufficiently off shell, $|\omega - p| \gtrsim gT$: indeed, the plasmons propagate as massive particles, with (momentum dependent) thermal masses of order gT [17,6,16].

(ii) The contributions involving β_l and β_t describe collisional damping, where the fermion exchanges a virtual photon with the other charged particles of the plasma. Such processes have no kinematical restrictions, and they are the only one to contribute at very large times $t \gg 1/gT$.

To study the large-time behavior, we restrict therefore ourselves to collisional processes, i.e., retain only β_l and β_t in the photon spectral functions. Also, we replace $H(q_0) \simeq T/q_0$, as appropriate for soft $q_0 \ll T$. From perturbation theory, we know that the infrared complications are related to the singular behavior of the magnetic spectral density as $q_0 \ll q \to 0$ [8]:

$$\frac{1}{q_0}\,\beta_t(q_0 \ll q) \simeq \frac{3\pi}{2}\,\frac{\omega_p^2 q}{q^6+(3\pi\omega_p^2 q_0/4)^2} \to \frac{2\pi}{q^2}\,\delta(q_0) \quad \text{as} \quad q\to 0. \tag{3.3}$$

To isolate this singular behavior, we write

$$\frac{1}{q_0}\,\beta_t(q_0,q) \equiv 2\pi\delta(q_0)\left(\frac{1}{q^2}-\frac{1}{q^2+\omega_p^2}\right)+\frac{1}{q_0}\,\nu_t(q_0,q). \tag{3.4}$$

A contribution $\propto 1/(q^2+\omega_p^2)$ has been subtracted from the singular piece—and implicitly included in $\nu_t(q_0,q)$—to avoid spurious ultraviolet divergences: written as they stand, both terms in the right-hand side (RHS) of Eq. (3.4) give UV-finite contributions. Note that by neglecting the regular piece $\nu_t(q_0,q)$ in the right-hand side of Eq. (3.4), one recovers our previous result in Refs. [7, 8] [as also expressed in Eqs. (3.6) and (3.9) below].

With Eq. (3.4), the integral in Eq. (2.25) may be separated into two pieces:

$$F_{\rm reg}(t) \equiv \int \frac{d^3q}{(2\pi)^3}\int_{-q}^{q}\frac{dq_0}{2\pi q_0}\,[\beta_l(q_0,q)-\cos^2\theta\,\beta_t(q_0,q) + \nu_t(q_0,q)]\,\frac{1-\cos t(v\cdot q)}{(v\cdot q)^2}, \tag{3.5}$$

and

$$F_{\rm IR}(t) \equiv \int \frac{d^3q}{(2\pi)^3}\left(\frac{1}{q^2}-\frac{1}{q^2+\omega_p^2}\right)\frac{1-\cos t(\mathbf{v}\cdot\mathbf{q})}{(\mathbf{v}\cdot\mathbf{q})^2}. \tag{3.6}$$

The first piece, $F_{\rm reg}(t)$, is infrared safe, and its large-time limit can be taken by replacing $f(t,v\cdot q)$ by $\pi t\,\delta(v\cdot q)$ [see Eq. (2.27)]. This yields

$$F_{\rm reg}(t) \equiv \frac{t}{4\pi}\int_0^\infty dq\; q\int_{-q}^{q}\frac{dq_0}{2\pi q_0}\left(\beta_l(q_0,q)-\frac{q_0^2}{q^2}\,\beta_t(q_0,q) + \nu_t(q_0,q)\right), \tag{3.7}$$

where we have used the delta function $\delta(q_0-q\,\cos\theta)$ to perform the angular integration. The remaining integral occurs also in Ref. [11], as part of the one-loop damping rate, and was computed there by using sum rules plus numerical integration. It is computed analytically in Appendix B, with the result

$$F_{\rm reg}(t) = \frac{t}{8\pi}\,\ln 3 \simeq \frac{t}{4\pi}\times 0.54931. \tag{3.8}$$

Note that this result comes entirely from the electric piece $\beta_l(q_0,q)$: the two magnetic pieces $(q_0^2/q^2)\beta_t(q_0,q)$ and $\nu_t(q_0,q)$, happen to cancel each other in the final result. This is purely accidental, consequence of our specific choice for the substracted term $1/(q^2+\omega_p^2)$ in Eq. (3.4).

The second piece, $F_{\rm IR}(t)$, contains the potentially singular magnetic contribution, so that we should take the large time limit only after performing the integral over q. This has been done in Ref. [8], with the following result (γ_E is the Euler constant):

$$F_{\rm IR}(t)=\frac{t}{4\pi}\,[\ln\omega_p t+(\gamma_E-1)+O(1/\omega_p t)]. \tag{3.9}$$

Note that the energy scale ω_p inside the logarithm arises from the large momentum ($q\gtrsim gT$) behavior, where the subtracted term $1/(q^2+\omega_p^2)$ acts effectively as an UV cutoff.

The final result for the large-time propagator reads then

$$\Delta(t\gg 1/\omega_p)\simeq\exp\{-\alpha T t[\ln(\omega_p t)+0.12652\ldots +O(g,1/\omega_p t)]\}. \tag{3.10}$$

For the consistency of our approximations, it is important to observe that this result has been obtained by integrating, in Eqs. (3.7) and (3.6), over soft photon momenta $q\lesssim gT$. While this is obvious for Eq. (3.6), where the two terms inside the parentheses mutually cancel as $q\gg gT$, it can be also verified for Eq. (3.7), by using the known behavior of β_l and β_t at large photon momenta [18,8].

For completeness, let us also give the corresponding results for a massive test particle. After reinserting the appropriate factors of $v\equiv|\mathbf{v}|$ in the previous results, we get

$$\Delta_v(vt\gg 1/\omega_p)\simeq\exp\{-\alpha T v t[\ln(\omega_p v t)+(\gamma_E-1)+C(v)]\}, \tag{3.11}$$

where $C(v)$ is given by the following integral:

$$C(v)=\frac{1}{v^2}\int_0^\infty dq\; q\int_{-vq}^{vq}\frac{dq_0}{2\pi q_0}\left(\beta_l(q_0,q)-\frac{q_0^2}{q^2}\,\beta_t(q_0,q)+v^2\nu_t(q_0,q)\right). \tag{3.12}$$

For a very heavy particle $m\gtrsim T$, we may consider the nonrelativistic limit $v\ll 1$ (this is consistent with our approximations as long as $p\cong mv\gg gT$). At small v, the leading contribution to Eq. (3.12) comes from the electric sector. The magnetic contribution involves a supplementary factor of v^2, and vanishes as $v\to 0$. However, because of its infrared sensitivity, the contribution of the magnetic sector is not analytic in v. We evaluate this contribution in Appendix B, where we find

$$vC(v)=\frac{1}{2}\left(1+v\,\ln\frac{3\pi v}{4}+\frac{v}{2}+O(v^2)\right), \tag{3.13}$$

where the first term, independent of v, is the contribution of the electric sector. Together with Eq. (3.11), this yields

$$\Delta_v(vt\gg 1/\omega_p)\simeq\exp\left\{-\frac{\alpha T}{2}\,t\left[1+v\,\ln\left(\frac{3\pi}{4}\,v^3(\omega_p t)^2\right)+v(2\gamma_E-3/2)\right]\right\}, \tag{3.14}$$

for $v\ll 1$. In particular, as $v\to 0$ (i.e., $m\to\infty$), the damping is purely exponential, with a damping rate $\gamma_0=\alpha T/2$ which coincides with the one-loop result in Ref. [9]. As for the v-dependent terms, the coefficient of the logarithm in Eq. (3.14) is the same as for the infrared-divergent piece of the corresponding one-loop result.[1]

IV. GAUGE DEPENDENCE

We show now that the same result (3.10) is obtained in general covariant gauges provided the large time limit in Eq. (2.25) is taken with an infrared cutoff in the gauge sector, in order to eliminate the contribution of the spurious degrees of freedom.

In the covariant gauge of Eq. (2.11), the photon spectral density reads

$$\widetilde{\rho}(q_0,\mathbf{q})=\left(\frac{q^2-q_0(\mathbf{v}\cdot\mathbf{q})}{q^2-q_0^2}\right)^2\rho_l(q_0,q)+[1-(\mathbf{v}\cdot\hat{\mathbf{q}})^2]\rho_t(q_0,q)+\lambda\rho_\lambda(q_0,\mathbf{q}). \tag{4.1}$$

The longitudinal and transverse spectral functions ρ_l and ρ_t are the same as in Eq. (3.1), and

$$\rho_\lambda(q_0,\mathbf{q})\equiv(q_0-\mathbf{v}\cdot\mathbf{q})^2 2\pi\epsilon(q_0)\delta'(q^2), \tag{4.2}$$

where $\epsilon(q_0)\equiv\theta(q_0)-\theta(-q_0)$ and $\delta'(q^2)$ is the derivative of $\delta(q^2)$ with respect to q^2.

The electric and magnetic spectral functions in Eq. (4.1) yield the same contributions to Eq. (2.25) as the corresponding functions in the Coulomb gauge [cf. Eqs. (3.6) and (3.8)]. This is obvious for the magnetic sector. In the electric sector, the large-time limit introduces the delta function $\delta(v\cdot q)$ [see Eq. (2.27)], and the projection factor multiplying $\rho_l(q_0,q)$ in Eq. (4.1) is equal to one for $q_0=\mathbf{v}\cdot\mathbf{q}$. The same argument applied in the gauge sector seems to imply that the contribution of $\rho_\lambda(q_0,q)$ does also vanish, because of the factor $(q_0-\mathbf{v}\cdot\mathbf{q})^2$ in Eq. (4.2). However, since the spectral function $\delta'(q^2)$ has support precisely at the integration limits $q_0=\pm q$, we should be more careful when taking the limit $v\cdot q\to 0$.

The contribution of the gauge sector to $\Delta(t)$ factorizes as $\exp[-\lambda g^2 T F_\lambda(t)]$, where

$$F_\lambda(t)\equiv\int\frac{d^3q}{(2\pi)^3}\int\frac{dq_0}{2\pi q_0}\,\rho_\lambda(q_0,\mathbf{q})\,\frac{1-\cos t(v\cdot q)}{(v\cdot q)^2}=\int\frac{d^3q}{(2\pi)^3}\int\frac{dq_0}{q_0}\,\epsilon(q_0)\delta'(q^2)[1-\cos t(v\cdot q)]. \tag{4.3}$$

By noting that $\delta'(q^2)=(1/2q_0)(d\delta/dq_0)$, we can perform an integration by parts to compute the integral over q_0. After also computing the angular integral, we obtain

$$F_\lambda(t)=\frac{1}{2\pi^2}\int_\mu^\infty\frac{dq}{q^2}\left\{1-\frac{\sin 2qt}{2qt}-\frac{1-\cos 2qt}{4}\right\}. \tag{4.4}$$

[1]Actually, a different coefficient was reported in Refs. [9,11], but the difference is apparently due to an error in the calculations there.

Although this last integral is infrared finite, we nevertheless compute it with an infrared cutoff μ. A straightforward calculation then yields

$$F_\lambda(t)=\frac{1}{8\pi^2\mu}\left[3-2\,\frac{\sin 2\mu t}{2\mu t}-\cos 2\mu t\right]-\frac{t}{4\pi^2}\,\mathrm{si}(2\mu t), \tag{4.5}$$

where $\mathrm{si}(x)\equiv-\int_x^\infty dz(\sin z/z)$ is the sine integral function [19].

If we remove the IR cutoff by letting $\mu\to 0$ at fixed t, then, by using $\mathrm{si}(0)=-\pi/2$, we get

$$F_\lambda(t)=\frac{t}{8\pi}, \tag{4.6}$$

so that $\Delta(t)$ becomes [cf. Eq. (3.10)]

$$\Delta(t\gg 1/\omega_p)\simeq\exp\{-\alpha T t[\ln(\omega_p t)+0.12652\cdots+\lambda/2]\}. \tag{4.7}$$

(The gauge-dependent piece in the exponent coincides with the corresponding piece of the one-loop damping rate, $\gamma_\lambda=\lambda\alpha T/2$ [20,21].)

However, if we consider the large-time behavior at fixed μ, then we can use the asymptotic expansion of $\mathrm{si}(x)$, that is

$$-\mathrm{si}(x\gg 1)\sim\frac{1}{x}\left(\cos x+\frac{\sin x}{x}+O(1/x^2)\right), \tag{4.8}$$

to obtain

$$F_\lambda(t\gg 1/\mu)=\frac{1}{8\pi^2\mu}\left[3-\frac{\sin 2\mu t}{2\mu t}+O(1/\mu^2t^2)\right]. \tag{4.9}$$

In this case, the sole effect of the gauge-dependent piece $F_\lambda(t)$ at times $t\gg 1/\mu$ is to change the normalization of the propagator, by a factor

$$\exp[-\lambda g^2 T F_\lambda(t)]\simeq\exp\left(-\lambda\,\frac{3\alpha}{2\pi}\,\frac{T}{\mu}\right)\equiv z(T,\mu,\lambda), \tag{4.10}$$

which is both gauge dependent and cutoff dependent.

The gauge-dependent contribution to the damping rate, Eq. (4.6), arises because the on-shell fermion is kinematically allowed to ''decay'' with the emission, or the absorption, of a massless gauge ''photon.'' At $T=0$, such an emission process cannot occur: by kinematics, the emitted photon must be colinear ($\theta=0$, $q_0=q$), and the corresponding phase space vanishes. But this is not so at finite temperature, because of the Bose-Einstein factor $N(q_0)\sim T/q_0$ which diverges as $q_0\to 0$ (see Appendix B of Ref. [8] for an explicit calculation). After HTL resummation, the gauge sector is the only one to contain massless fields. The unphysical decay channel can be suppressed by giving the gauge photon a small mass μ, as originally proposed by Rebhan [21] (see also Refs. [22, 23]). As we have seen, this procedure ensures the gauge independence of the damping rate, to the order of interest.

Further insight may be gained by a comparison with the corresponding results at zero temperature [2]. After ultraviolet renormalization, the retarded BN propagator at zero temperature is given by

$$S(t,\mathbf{p})\propto e^{-iE_p t}\exp\left\{(3-\lambda)\,\frac{\alpha}{2\pi}\ln(mt)\right\}$$
$$=(mt)^{(3-\lambda)(\alpha/2\pi)}e^{-iE_p t}. \tag{4.11}$$

Thus, in the energy representation, the mass-shell singularity is generally a branch point, rather than a simple pole:

$$S(p)\propto\frac{1}{u\cdot p-m}\left(\frac{m}{u\cdot p-m}\right)^{(3-\lambda)(\alpha/2\pi)}, \tag{4.12}$$

where $u^\mu=(u_0,\mathbf{u})$ is the fermion four-velocity $u^\mu=p^\mu/m$, with $u^2=1$.

Note that both the physical and the gauge sectors of the photon propagator contribute to the mass-shell behavior in Eq. (4.12): at $T=0$, the gauge field quanta are massless in both sectors. Furthermore, no infrared regulator is necessary: in deriving Eqs. (4.11)–(4.12), one encounters no IR divergences, and the position of the mass shell is gauge independent, as it should. Still, if one wishes to perform soft-photon computations in perturbation theory in any other gauge than the Yennie gauge ($\lambda=3$), it is convenient to introduce an infrared regulator, so as to recover the simple-pole structure of the mass shell. When the photon is given a small mass μ, the propagator (4.12) is replaced by

$$S(p)\propto\frac{z(\mu,\lambda)}{u\cdot p-m}, \tag{4.13}$$

where the residue

$$z(\mu,\lambda)=\exp\left\{(3-\lambda)\,\frac{\alpha}{2\pi}\ln(m/\mu)\right\}, \tag{4.14}$$

is gauge-fixing dependent and also cutoff-dependent. It may be compared to the finite-temperature normalization factor in Eq. (4.10).

We see that, as a consequence of the Bose-Einstein enhancement of the soft photon processes, the divergence of the ''residue'' $z(T,\mu,\lambda)$ as $\mu\to 0$ is linear at $T>0$, rather than just logarithmic at $T=0$. Moreover, if at $T=0$ the introduction of a photon mass is just a matter of convenience, at $T>0$ the use of an infrared regulator in the gauge sector is compulsory in order to eliminate the contribution of the nonphysical degrees of freedom and avoid the gauge dependence of the mass shell.

V. SOME RESULTS FOR QCD

We consider now the generalization of the previous arguments to the non-Abelian case, that is, to the high-temperature, weakly coupled [$g(T)\ll 1$] quark-gluon plasma. The self-interactions of the soft gluons prevent us from getting in this case an explicit solution. However, it is expected [24] that these interactions generate screening of the static magnetic fields. If this is so, the corresponding screening length, typically of order $1/g^2T$, provides then a

natural IR cutoff of order g^2T in the perturbation theory for γ.

We shall investigate this possibility in the next subsection, in the framework of a toy model which is QED with an infrared cutoff $\mu \sim g^2T$ in the magnetic sector. By solving this model in the BN approximation, we shall obtain a qualitative picture of the effects of the magnetic mass on the large-time behavior of the fermion propagator.

Then, we shall propose a functional integral representation for the propagator of a hard quark or gluon which, being formulated in three-dimensional Euclidean space, is *a priori* well suited for lattice calculations. This formulation allows for a direct numerical study of the particle decay in real time.

A. QED with a magnetic mass

To implement magnetic screening in QED, we replace the massless static transverse propagator by its massive version

$$D_{ij}(0,\mathbf{q}) = \frac{\delta_{ij} - \hat{q}_i \hat{q}_j}{q^2 + \mu^2}, \tag{5.1}$$

with $\mu \sim g^2T$. Of course, such an infrared behavior could not occur in QED, where the correct magnetic polarization tensor $\Pi_t(0,q)$ vanishes as q^2 when $q \to 0$, to all orders in perturbation theory [25]. We simply use ''massive QED,'' as defined by Eq. (5.1), as a crude parametrization of the nonperturbative screening effects in QCD.

Strictly speaking, when $\mu > 0$ we have no infrared divergences. However, as long as $\mu \lesssim g^2T$, the dominant contribution to the damping rate is still given by the static magnetic photons. For instance, to one loop order the static mode yields

$$\gamma_{\rm st} = \alpha T \ln \frac{\omega_p}{\mu} \sim g^2 T \ln(1/g), \tag{5.2}$$

which is enhanced by a factor $\ln(1/g)$ as compared to the contribution of the nonstatic modes [which is $\sim g^2T$, as in Eq. (3.10)]. Moreover, the higher-loop diagrams contribute terms of relative order $(\alpha T/\mu)^{n-1}$, where n is the number of loops, so that the perturbation theory breaks down for $\mu \lesssim g^2T$ [8]. This is why a nonperturbative calculation is necessary even in the presence of an infrared cutoff $\mu \lesssim g^2T$.

In order to get the leading contribution to the damping factor, we can restrict ourselves to the interactions with static $(q_0 = 0)$ magnetic photons [7,8]. In practice, such a calculation amounts to preserve only the contribution $F_{\rm IR}(t)$ in Eq. (3.6), where however, the massive propagator (5.1) must now be used. This gives

$$\Delta_\mu(t) \simeq \exp\left\{ -g^2T \int \frac{d^3q}{(2\pi)^3} \frac{1}{q^2+\mu^2} \frac{1-\cos t(\mathbf{v}\cdot\mathbf{q})}{(\mathbf{v}\cdot\mathbf{q})^2} \right\}. \tag{5.3}$$

As explained in Sec. III, the integral in Eq. (5.3) has to be computed with an upper cutoff $\omega_p \sim gT$, to account approximately for the effect of the neglected nonstatic modes. (In Eq. (3.6), the upper cutoff was provided by the subtracted term $1/(q^2+\omega_p^2)$. In Eq. (5.4) below, we shall find convenient to introduce this cutoff in a different way. At large times $\omega_p t \gg 1$, the leading contribution to the damping factor is indeed insensitive to the precise value of the UV cutoff, and also to the specific procedure which is used for its implementation [8].)

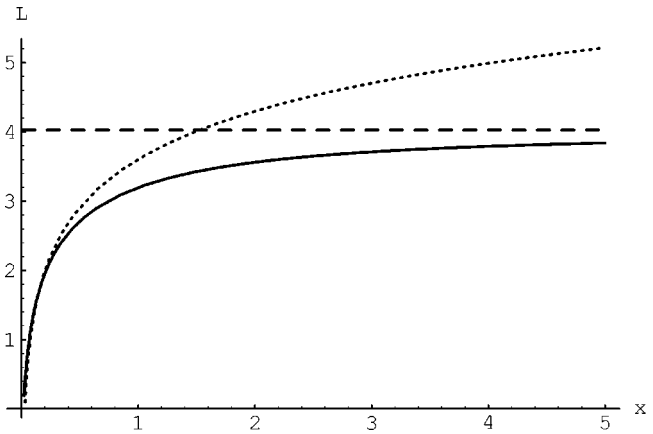

FIG. 3. The function $L(x,y)$, Eq. (5.5), is represented as a function of x for fixed $y = 0.01$ (continuous line). We have also represented the asymptotics $L_1(x,y) \equiv \ln(x/y) - 1$ (dotted line) and $L_2(x,y) \equiv \ln(1/y) - \gamma_E$ (dashed line). These are good approximations to $L(x,y)$ in the domains $y \ll x \ll 1$ and $x \gg 1$, respectively.

To perform the integral in Eq. (5.3), we write $\Delta_\mu(t) = \exp[-g^2TF_\mu(t)]$, with

$$\begin{aligned} F_\mu(t) &= \frac{1}{2} \int_0^t ds_1 \int_0^t ds_2 \int \frac{d^3q}{(2\pi)^3} \frac{e^{i(\mathbf{v}\cdot\mathbf{q})(s_1-s_2)}}{q^2+\mu^2} \\ &= \frac{1}{8\pi} \int_0^t ds_1 \int_0^t ds_2 \, \frac{e^{-\mu|s_1-s_2|}}{|s_1-s_2|} \, \theta(|s_1-s_2| - 1/\omega_p) \\ &= \frac{1}{4\pi} \int_{1/\omega_p}^t ds \, \frac{t-s}{s} \, e^{-\mu s} \\ &= \frac{t}{4\pi} \left\{ \int_{\mu/\omega_p}^{\mu t} \frac{dx}{s} \, e^{-x} - \frac{e^{-\mu/\omega_p} - e^{-\mu t}}{\mu t} \right\}. \end{aligned} \tag{5.4}$$

In this calculation, the ultraviolet cutoff has been introduced, in the second line, in the function $\theta(|s_1-s_2| - 1/\omega_p)$. For the purpose of a graphical representation (see Fig. 3), we rewrite the final expression above as $F_\mu(t) \equiv (t/4\pi) L(x,y)$, with $x \equiv \mu t$, $y \equiv \mu/\omega_p$, and

$$L(x,y) \equiv E_1(y) - E_1(x) - \frac{e^{-y} - e^{-x}}{x}, \tag{5.5}$$

where $E_1(x)$ is the exponential-integral function [19], $E_1(x) = \int_1^\infty dz (e^{-xz}/z)$. For $\mu \sim g^2T$, we have $y \sim g \ll 1$. We recall that the above calculation only makes sense for large enough times, $\omega_p t \gg 1$ or $x \gg y$.

Since the expression in Eq. (5.4) involves two energy scales, namely, ω_p and μ, with $\mu \ll \omega_p$, we distinguish between two regimes of time: (i) very large times, $t \gg 1/\mu$ (i.e., $x \gg 1$), where

$$F_\mu(t) \simeq \frac{t}{4\pi} \left(\ln \frac{\omega_p}{\mu} + O(1) \right), \tag{5.6}$$

and (ii) intermediate times, $1/\omega_p \ll t \ll 1/\mu$ (i.e., $y \ll x \ll 1$), where

$$F_\mu(t) \simeq \frac{t}{4\pi}\,[\ln(\omega_p t) + O(1)]. \tag{5.7}$$

Thus, the ''magnetic mass'' μ is only felt at sufficiently large times—where $\Delta_\mu(t)$ decays exponentially in agreement with the one-loop result (5.2)—while it has no effect at intermediate times. We remark at this point that, when discussing the lifetime of the excitation, it is rather the intermediate times which matter, since for asymptotically large times $t \gtrsim 1/g^2T \sim 1/\mu$ the excitation has already decayed. This behavior, Eqs. (5.6) and (5.7), can be also observed in Fig. 3, where we have represented $L(x,y)$ as a function of x for a fixed, small, value of y (namely, $y=0.01$). For x of order one, one clearly sees on this figure the transition between the two types of behavior, as described by Eqs. (5.6) and (5.7), respectively.

It has been suggested, first by Lebedev and Smilga [10], that when computing the damping rate to one-loop order, the damping rate itself should be self-consistently resummed in the internal hard line. The usual argument goes as follows. Since $\gamma \sim g^2T$ is of the same order as the infrared cutoff μ, it should be taken into account when studying the infrared behavior of the integrand. If we do that, by following Ref. [11], then the one-loop result (5.2) is modified to

$$\gamma \simeq \frac{\alpha T}{2}\,\ln\frac{\omega_p^2}{\mu^2 + 2\mu\gamma}. \tag{5.8}$$

(Up to appropriate color factors, the same result is obtained in QCD, for both quarks and gluons [11].) However, this is not correct: the self-energy resummation advocated in the procedure leading to Eq. (5.8) should be accompanied by a corresponding resummation in the vertex function, so as to respect gauge symmetry. As discussed in Ref. [8], the vertex corrections generate new infrared divergences, and, when added to the self-energy corrections, conspire to give a leading-order estimate for the damping rate which has precisely the form indicated in Eq. (5.2). (See Appendix C in Ref. [8] for more details.) At this point, it might be useful to emphasize that the BN calculation provides precisely a self-consistent resummation of the fermion propagator near the mass shell, together with the appropriate resummation of the vertex function, as required by gauge symmetry.

B. QCD

Going now to QCD, we first observe that the Bloch-Nordsieck approximation remains relevant to discuss the large-time (or mass-shell) behavior of the quasiparticle propagator, and this for both quarks and (transverse) gluons. (We consider here a hard quasiparticle, with momentum $p \gtrsim T$.) While for quarks this approximation is easy to justify, by analogy to QED, the case of gluons requires more care and is discussed in Appendix C. Moreover, we expect the leading large-time behavior to be given by the quasiparticle interactions with static ($q_0=0$) and very soft ($q \to 0$) magnetic gluons: indeed, these are the interactions which generate the infrared divergences of the perturbation theory [8].

What is new with respect to QED, is that the relevant self-energy corrections also include the mutual interactions of the internal gluons, expected, in particular, to lead to magnetic screening. A typical Feynman graph contribution to the self-energy is depicted in Fig. 4. The continous line in this diagram is hard, and may represent either a quark, or a gluon. The wavy lines denote static magnetic gluons, and all the loop integrations are three-dimensional. As explained in Sec. III, these integrations involve an upper cutoff ω_p. In QCD [6],

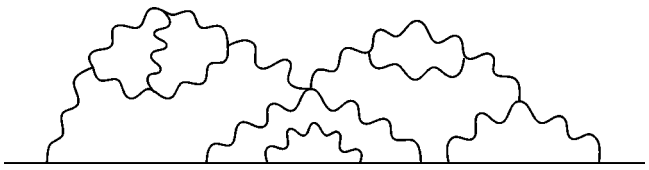

FIG. 4. A generic self-energy diagram in QCD which yields infrared divergences on the mass shell. The continuous line is a hard particle (quark or gluon). The wavy lines are soft magnetostatic gluons. All the loop integrations are three dimensional.

$$\omega_p^2 = \frac{g^2T^2}{18}\,(2N + N_f), \tag{5.9}$$

for N colors and N_f flavors of thermal quarks. (Note that the gluonic loops attached to soft internal lines would be finite even in the absence of the ultraviolet cutoff.)

In the BN approximation, all such diagrams are formally resummed by the following functional integral [the gauge-fixing terms are not written here explicitly; see the discussion below, after Eq. (5.14)]:

$$S(x-y) = Z^{-1}\int \mathcal{D}\mathbf{A}\,G(x,y|\mathbf{A})\exp\left\{-\frac{1}{4T}\int d^3x F_{ij}^a F_{ij}^a\right\}, \tag{5.10}$$

where $\mathbf{A}^a(\mathbf{x})$ is a static color field, $F_{ij}^a = \partial_i A_j^a - \partial_j A_i^a - g f^{abc} A_i^b A_j^c$ (f^{abc} are the structure constants of the color group), and $G(x,y|\mathbf{A})$ satisfies the equation

$$i(v\cdot D_x)\,G(x,y|\mathbf{A}) = \delta^{(4)}(x-y), \tag{5.11}$$

where $D_\mu = \partial_\mu + igA_\mu$, $A_\mu = (0,\mathbf{A})$, and $A_i \equiv A_i^a T^a$ is a color matrix in either the adjoint or the fundamental representation (for gluons or quarks, respectively). The plasma effects do not modify the gluonic action in Eq. (5.10) (recall that the HTL corrections vanish for static magnetic fields [4]), but only enter through the upper cutoff $\omega_p \sim gT$.

The solution of the BN equation (5.11) with retarded boundary conditions is immediate [6]:

$$G_R(x,y|\mathbf{A}) = -i\,\theta(x_0-y_0)\,\delta^{(3)}[\mathbf{x}-\mathbf{y}-\mathbf{v}(x_0-y_0)]\,U(\mathbf{x},\mathbf{y}),$$

$$U(\mathbf{x},\mathbf{x}-\mathbf{v}t) = P\,\exp\left\{ig\int_0^t ds\;\mathbf{v}\cdot\mathbf{A}[\mathbf{x}-\mathbf{v}(t-s)]\right\}, \tag{5.12}$$

where the path-ordering operator P is necessary since the color matrices $\mathbf{A}(\mathbf{x})$ at different points along the path do not commute with each other.

The retarded propagator $S_R(x-y)$ is calculated by inserting Eq. (5.12) in the functional integral (5.10). It can be written as

$$S_R^{ab}(t,\mathbf{p}) = -i\,\delta^{ab}\,\theta(t)\,e^{-it(\mathbf{v}\cdot\mathbf{p})}\,\Delta(t), \tag{5.13}$$

with

$$\Delta(t) \equiv \mathcal{N}\int \mathcal{D}\mathbf{A}\ \mathrm{Tr}\ U(\mathbf{x},\mathbf{x}-\mathbf{v}t)\exp\left\{-\frac{1}{2T}\int d^3x\ \mathbf{B}^2\right\}, \tag{5.14}$$

$\mathbf{B}^2 = B_i^a B_i^a$, and $B_i^a = (1/2)\epsilon_{ijk}F_{jk}^a$ is the chromomagnetic field. In order for Eq. (5.14) to be well defined, it is further necessary to choose a gauge within the functional integral. [Recall that the parallel transporter $\mathrm{Tr}U(\mathbf{x},\mathbf{x}-\mathbf{v}t)$ is not invariant under the gauge transformations of the background color field.] However, we shall argue below that the dominant large-time behavior should be independent of the gauge-fixing condition.

The functional integral (5.14) cannot be computed analytically because $\mathbf{B}^a$ is nonlinear in the gauge potentials. However, we may expect the large-time behavior of $\Delta(t)$ to be similar to that of the model discussed in Sec. V A, that is [cf. Eqs. (5.6) and (5.7)],

$$\Delta(1/\omega_p \ll t \ll 1/\mu) \simeq \exp\left\{-C_r\,\frac{g^2T}{4\pi}\,t[\ln(\omega_p t)+O(1)]\right\}, \tag{5.15}$$

at intermediate times, and, respectively,

$$\Delta(t \gg 1/\mu) \simeq \exp\left\{-C_r\,\frac{g^2T}{4\pi}\,t\left(\ln\frac{\omega_p}{\mu}+O(1)\right)\right\}, \tag{5.16}$$

at very large times. In these equations, C_r is the Casimir factor of the appropriate color representation [i.e., $C_q=(N^2-1)/2N$ for a hard quark, and $C_g=N$ for a hard gluon], and the magnetic mass $\mu\sim g^2T$ is expected to come out from the soft gluon mutual interactions. Note that the order 1 terms in the above equations are not consistently determined by the present approximation: Indeed, from the experience with QED, and also from the one-loop calculations in QCD [10–12], we know that such terms receive contributions from the non-static gluon modes, and that they may be sensitive to the gauge-fixing condition (see Sec. IV).

To verify this picture, one could rely on a lattice computation of the Euclidean functional integral (5.14). The parallel transporter $\mathrm{Tr}U(\mathbf{x},\mathbf{x}-\mathbf{v}t)$ is easily implemented as a product of link operators. [Recall that $\mathbf{v}$ is a fixed unit vector, e.g., $\mathbf{v}=(0,0,1)$, so that $U(\mathbf{x},\mathbf{x}-\mathbf{v}t)$ is a product of link operators in the z direction, from z_0-t to z_0, with z_0 an arbitrary site on the lattice.] Since the expression (5.14) is defined with an upper cutoff $\omega_p\sim gT$, the lattice spacing a is fixed: $a\sim 1/\omega_p$. From perturbation theory, we expect the decay of $\Delta(t)$ at times $t\gg a$ to be only logarithmically sensitive to the precise value of a [cf. Eqs. (5.15) and (5.16)].

The objective of a lattice calculation would be then to verify the large-time behavior predicted in Eqs. (5.15) and (5.16). By observing the interplay between these two regimes, one may verify what is the typical scale for the emergence of magnetic screening: indeed, we expect the transition between two regimes to occur for $t\sim 1/\mu$. However, this could not be sufficient for a quantitative measure of the magnetic mass, because of the theoretical uncertainty on the subleading term of order 1.

The main limitation against an explicit calculation comes from the lattice size: indeed, in order to verify the aforementioned picture, one needs a small coupling constant $g\ll 1$—to ensure a clean separation between the scales g^2T and gT—together with large values of time, up to $t_{\max}\gg 1/g^2T\sim a/g$. Thus, the lattice should have at least N^3 sites, with $N\gtrsim t_{\max}/a\gg 1/g$.

VI. CONCLUSIONS

In this paper, we have completed the analysis of the Bloch-Nordsieck propagator in hot QED, and we have also discussed the usefulness of such an approximation for a high-temperature QCD plasma.

As compared to Refs. [7,8], several points have been clarified by the present analysis. First, the three-dimensional model of [7,8] suffers from a spurious ultraviolet divergence coming from the restriction to the static photon mode. We have shown here that the contribution of the nonstatic modes provides a dynamical cutoff at momenta $\sim gT$. Not only this justifies the cutoff procedure used in Refs. [7,8], but it also allows one to compute explicitly the subleading term in the large time behavior [cf. Eq. (3.10)].

Secondly, the effects of the gauge-fixing procedure only enter at the level of the subleading term. Thus, by computing this term in different gauges, one can study the gauge (in) dependence of the large-time decay. We have performed this computation in the Coulomb gauge, and in a generic covariant gauge, with conclusions which agree with the one-loop calculations in Refs. [20,21]; namely, the subleading term is gauge independent if computed in the presence of an infrared cutoff in the gauge sector. Physically, such a cutoff separates the particle mass shell from the threshold for the spurious emission or absorption of massless gauge photons. With a nonzero infrared regulator μ, the gauge-dependent contribution to the damping vanishes in a vicinity $\sim\mu$ of the mass shell or, equivalently, for times $t\gg 1/\mu$. Thus, to avoid spurious gauge contributions over a particle lifetime, one should choose $\mu\gtrsim\gamma$, where $\gamma\sim g^2T\ln(1/g)$.

Concerning QCD, we have argued that the BN model may still be a relevant approximation for the study of the quasiparticle mass shell. As compared to QED, the non-Abelian model is complicated by the soft gluon self-interactions. The problem simplifies considerably when one considers only the dominant contribution due to the static magnetic gluon modes: then, not only all the HTL corrections vanish, but the needed path integral can in principle be computed on a three-dimensional lattice, with a fixed lattice spacing $a\sim 1/gT$.

ACKNOWLEDGMENTS

It is a pleasure to thank S. Belyaev, A. Krasnitz, L. McLerran, J.-Y. Ollitrault, and B. Vanderheyden for discussions and useful remarks on the manuscript. Service de Physique Théorique is Laboratoire de la Direction des Sciences de la Matière du Commissariat à l'Energie Atomique.

APPENDIX A

In this appendix, we construct the BN propagator for a thermal fermion with momentum $p\sim T$. The final result turns out to be essentially the same as that obtained in Sec. III in the case $p\gg T$.

We use the imaginary-time formalism which has been developed in Ref. [8]. In this formalism, we have to solve the imaginary-time BN equation [cf. Eq. (2.10)]

$$-(v\cdot D_x)G(x,y|A)=\delta_E(x,y), \tag{A1}$$

with antiperiodic boundary conditions [cf. Eq. (2.14)]

$$G_E(\tau_x=0,\tau_y|A)=-G_E(\tau_x=\beta,\tau_y|A), \tag{A2}$$

and similarly for τ_y. In these equations, the time variables are purely imaginary [$x_0=t_0-i\tau_x$ and $y_0=t_0-i\tau_y$, with $0\leqslant\tau_x,\ \tau_y\leqslant\beta$ and $\delta_E(x-y)=\delta(\tau_x-\tau_y)\,\delta(\mathbf{x}-\mathbf{y})$], and the gauge fields are periodic in imaginary time: $A_\mu(\tau=0)=A_\mu(\tau=\beta)$. In Ref. [8], we have solved this equation explicitly in perturbation theory, i.e., as a series in powers of gA, and then we have performed the functional integration over the gauge fields [cf. Eq. (2.9)]. The resulting propagator can be written as [cf. Eq. (2.5)]

$$iS(x_0-y_0,\mathbf{p})=\theta(\tau)S^>(\tau,\mathbf{p})-\theta(-\tau)S^<(\tau,\mathbf{p}), \tag{A3}$$

where the analytic functions $S^>$ and $S^<$ are obtained in the form [8]

$$\begin{aligned} S^<(\tau,\mathbf{p})&=e^{-\tau E_p}\widetilde{V}(E_p;u=-\tau)\quad \text{for } -\beta\leqslant\tau\leqslant 0,\\ S^>(\tau,\mathbf{p})&=e^{(\beta-\tau)E_p}\widetilde{V}(E_p;u=\beta-\tau)\quad \text{for } 0\leqslant\tau\leqslant\beta. \end{aligned} \tag{A4}$$

In this equation, $E_p\equiv\mathbf{v}\cdot\mathbf{p}$ is the BN mass-shell and the function $\widetilde{V}(E_p;u)$ is given, for $0\leqslant u\leqslant\beta$, as a formal series in powers of g^2 [8]:

$$\begin{aligned} \widetilde{V}(E_p;u)=n(\mathbf{v}\cdot\mathbf{p})+\sum_{n\geqslant 1}(-1)^n\frac{g^{2n}}{n!}\int[dq_1dq_2\ldots dq_n]\frac{\widetilde{D}(q_1)\widetilde{D}(q_2)\cdots\widetilde{D}(q_n)}{(v\cdot q_1)^2(v\cdot q_2)^2\cdots(v\cdot q_n)^2}\{n(\mathbf{v}\cdot\mathbf{p})-n[\mathbf{v}\cdot(\mathbf{p}+\mathbf{q}_1)]e^{-u(v\cdot q_1)}\\ -n[\mathbf{v}\cdot(\mathbf{p}+\mathbf{q}_2)]e^{-u(v\cdot q_2)}+\cdots+(-1)^n n[\mathbf{v}\cdot(\mathbf{p}+\mathbf{q}_1+\mathbf{q}_2+\cdots+\mathbf{q}_n)]e^{-uv\cdot(q_1+q_2+\cdots+q_n)}\}, \end{aligned} \tag{A5}$$

with $\widetilde{D}(q)\equiv v^\mu{}^*D_{\mu\nu}(i\omega_m,\mathbf{q})v^\nu$. In this and the following equations, the photon energies q_i^0 are discrete and purely imaginary: $q^0=i\omega_m=i2\pi mT$, with integer m (Matsubara frequencies). The measure in the momentum integrals is denoted by

$$\int[dq]\equiv T\sum_{\omega_m}\int\frac{d^3q}{(2\pi)^3}. \tag{A6}$$

The thermal factors make the momentum integrals in Eq. (A5), such as

$$\int\frac{d^3q}{(2\pi)^3}\,n[\mathbf{v}\cdot(\mathbf{p}+\mathbf{q})]e^{u(\mathbf{v}\cdot\mathbf{q})}, \tag{A7}$$

convergent for any $0<u<\beta$. This, in turn, ensures the analyticity of the functions $S^<(\tau)$ and $S^>(\tau)$ in Eq. (A4) [16]. By analytically continuing these functions toward the real-time axis (i.e., by replacing $\tau\to it$ with real t), one constructs the retarded propagator

$$\begin{aligned} S_R(t,\mathbf{p})&=-i\theta(t)[S^>(t,\mathbf{p})+S^<(t,\mathbf{p})]\\ &=-i\theta(t)e^{-itE_p}\{e^{\beta E_p}\widetilde{V}(E_p;u=\beta-it)\\ &\quad+\widetilde{V}(E_p;u=-it)\}. \end{aligned} \tag{A8}$$

Note, however, that the analytic continuation to real time can be done only after performing the Matsubara sums in all the terms of the series in Eq. (A5).

Fortunately, this can be done easily in the relevant regime of large time ($t\gg 1/gT$). According to the discussion in Sec. III, we expect then the momentum integrals to be dominated by soft photon momenta $q\lesssim gT$. Indeed, the photon propagator $\widetilde{D}(q)$, which can be rewritten as [with $\widetilde{\rho}(q)\equiv v^\mu\rho_{\mu\nu}(q)v^\nu$; cf. Eq. (3.1)]:

$$\widetilde{D}(i\omega_m,\mathbf{q})=\int_{-\infty}^{\infty}\frac{d\omega}{2\pi}\frac{\widetilde{\rho}(\omega,\mathbf{q})}{\omega-i\omega_m}, \tag{A9}$$

provides, through the spectral density $\widetilde{\rho}(\omega,\mathbf{q})$, an effective upper cutoff $\sim gT$ for the integrals over q. [Recall that the functions $\beta_l(\omega,q)$ and $\beta_t(\omega,q)$ in Eq. (3.2) are rapidly decreasing for $q\gg gT$.] Strictly speaking, this cutoff becomes effective only after u is continued to $\beta-it$ or $-it$. However, we may anticipate for its effect and supply the integrals over $\mathbf{q}_i$ in Eq. (A5) with an upper cutoff $\sim gT$. Then the photon momenta are limited to values $|\mathbf{q}|\ll|\mathbf{p}|\sim T$, and we can replace $n[\mathbf{v}\cdot(\mathbf{p}+\mathbf{q})]$ by $n(\mathbf{v}\cdot\mathbf{p})$ up to terms of order $q/T\lesssim g$. The fermion occupation factor $n(\mathbf{v}\cdot\mathbf{p})$ in Eq. (A5) then factorizes, and the resulting expression can be resummed into an exponential:

$$\begin{aligned} \widetilde{V}(E_p;u)&\approx n(E_p)\Delta^<(u),\\ \Delta^<(u)&\equiv\exp\left\{-g^2\int[dq]\widetilde{D}(q)\,\frac{1-e^{-u(v\cdot q)}}{(v\cdot q)^2}\right\}. \end{aligned} \tag{A10}$$

At this stage, we can then perform the Matsubara sum over $q^0=i\omega_m$ [by using the spectral representation in Eq. (A9), together with contour integration], and obtain

$$\Delta^<(u)=\exp\left\{-g^2\int\frac{d^4q}{(2\pi)^4}\,\widetilde{\rho}(q_0,\mathbf{q})\left[[1+N(q_0)]\times\frac{1-e^{-u(v\cdot q)}}{(v\cdot q)^2}-[1+N(\mathbf{v}\cdot\mathbf{q})]\,\frac{u}{v\cdot q}\right]\right\},\quad\text{(A11)}$$

where $v\cdot q=q_0-\mathbf{v}\cdot\mathbf{q}$ (we have renamed q_0 the real energy ω). The last expression can be now continued to $u\to -it$, with the result

$$\Delta^<(-it)\equiv\exp\left\{-g^2\int\frac{d^4q}{(2\pi)^4}\,\widetilde{\rho}(q)\left[[1+N(q_0)]\times\frac{1-e^{it(v\cdot q)}}{(v\cdot q)^2}+[1+N(\mathbf{v}\cdot\mathbf{q})]\,\frac{it}{v\cdot q}\right]\right\}$$
$$=\exp\{-it\Phi(t)\}\Delta(t),\quad\text{(A12)}$$

which involves the same functions $\Phi(t)$ and $\Delta(t)$ as in Sec. III [cf. Eqs. (2.24) and (2.25)]. At this point, the momentum integral in Eq. (A12) is ultraviolet finite and the cutoff can be removed. Recalling Eq. (A4), we can finally write

$$S^<(t,\mathbf{p})=e^{-itE_p}n(E_p)\Delta(t),\quad\text{(A13)}$$

where we have ignored the inconsistent phase $\Phi(t)$.

To compute $S^>(t,\mathbf{p})$, we start with [cf. the second Eq. (A4)]:

$$e^{\beta E_p}\widetilde{V}(E_p;u=\beta-\tau)\approx[1-n(E_p)]\Delta^>(\tau),$$

$$\Delta^>(\tau)\equiv\exp\left\{-g^2\int[dq]\widetilde{D}(q)\,\frac{1-e^{\tau(v\cdot q)}}{(v\cdot q)^2}\right\},\quad\text{(A14)}$$

where $1-n(E_p)\equiv e^{\beta E_p}n(E_p)$ has been factorized by the same approximations as above. After performing the Matsubara sum and the analytic continuation $\tau\to it$, we finally obtain [within the same accuracy as in Eq. (A13)]

$$S^>(t,\mathbf{p})=e^{-itE_p}[1-n(E_p)]\Delta(t).\quad\text{(A15)}$$

Thus, for sufficiently large times, both functions $S^<(t)$ and $S^>(t)$ decay as $\Delta(t)$, Eq. (2.25). The same is therefore true for the retarded propagator, as given by Eqs. (A8), (A13), and (A15):

$$|S_R(t,\mathbf{p})|\propto\Delta(t),\quad\text{(A16)}$$

which is the result quoted in Eq. (2.33).

APPENDIX B

In this appendix, we calculate the double integral in Eq. (3.7), thus proving the result quoted in Eq. (3.8). The method to be used here was suggested to us by Jean-Yves Ollitrault (see also [26]). We first write

$$I\equiv\int_0^\infty dq\;q\int_{-q}^{q}\frac{dq_0}{2\pi q_0}\times\left(\beta_l(q_0,q)-\frac{q_0^2}{q^2}\,\beta_t(q_0,q)+\nu_t(q_0,q)\right)$$
$$\equiv I_1+I_2+I_3,\quad\text{(B1)}$$

where the three pieces I_s, $s=1,2,3$, correspond to the three terms within the integrand. To illustrate the method, we compute the second piece in detail:

$$I_2=-\int_0^\infty dq\;q\int_{-q}^{q}\frac{dq_0}{2\pi q_0}\,\frac{q_0^2}{q^2}\,\beta_t(q_0,q)$$
$$=-\int_0^\infty\frac{dq}{q}\left\{1-2\int_q^\infty dq_0q_0\delta[q_0^2-q^2-\Pi_t(q_0,q)]\right\}.\quad\text{(B2)}$$

In going to the second line, we have used the familiar sum rule [16]

$$\int_{-\infty}^{\infty}\frac{dq_0}{2\pi}\,q_0\rho_t(q_0,q)=1,\quad\text{(B3)}$$

together with the parity property $\rho_t(-q_0,q)=-\rho_t(q_0,q)$, to write

$$\int_{-q}^{q}\frac{dq_0}{2\pi}\,q_0\beta_t(q_0,q)=1-2\int_q^\infty\frac{dq_0}{2\pi}\,q_0\rho_t(q_0,q);\quad\text{(B4)}$$

then we have related the on-shell magnetic spectral density to the plasmon pole in the transverse photon propagator $\rho_t(q_0>q)=2\pi\delta[q_0^2-q^2-\Pi_t(q_0,q)]$. We also recall that, in the hard thermal loop approximation, $\Pi_t(q_0,q)$ is a function of q_0/q alone.

The integral over q in Eq. (B2) is well defined as it stands. However, in order to work out separately the two terms within the braces, it is necessary to introduce, at intermediate steps, an ultraviolet cutoff Λ and also an infrared cutoff μ. The first term reads then

$$I_{21}(\Lambda,\mu)\equiv-\int_\mu^\Lambda\frac{dq}{q}=-\ln\frac{\Lambda}{\mu}.\quad\text{(B5)}$$

The second term

$$I_{22}(\Lambda,\mu)\equiv2\int_\mu^\Lambda\frac{dq}{q}\int_q^\infty dq_0q_0\delta[q_0^2-q^2-\Pi_t(q_0/q)],\quad\text{(B6)}$$

involves an integral along the transverse plasmon dispersion relation $q_0=\omega_t(q)$ with $\omega_t^2(q)=q^2+\Pi_t(\omega_t/q)$. To perform the integral, we use the following change of variables:

$$x\equiv q_0/q,\quad y\equiv q_0^2-q^2,\quad dq\;dq_0=\frac{dx\;dy}{2(x^2-1)},\quad\text{(B7)}$$

and get

$$I_{22}(\Lambda,\mu)=\int dx\int dy\ \frac{x}{x^2-1}\ \delta[y-\Pi_t(x)]=\int_{x_m}^{x_M}dx\ \frac{x}{x^2-1}$$
$$=\frac{1}{2}\ln\frac{x_M^2-1}{x_m^2-1}. \tag{B8}$$

The integration limits x_m and x_M are obtained as follows: As $q\to\mu$, $x\to\omega_t(\mu)/\mu$. The dispersion relation $\omega_t(q)$ can be found, e.g., in Refs. [18,6,16]. For $\mu\to 0$, $\omega_t(\mu)\to\omega_p$, and $x\to x_M(\mu)=\omega_p/\mu$. As $q\to\Lambda$ (with large $\Lambda\gg\omega_p$), $\omega_t^2(\Lambda)\simeq\Lambda^2+3\omega_p^2/2$, and $x\to x_m(\Lambda)=1+3\omega_p^2/4\Lambda^2$. Together with Eqs. (B5) and (B8), this gives

$$I_2=I_{21}+I_{22}=-\ln\frac{\Lambda}{\mu}+\frac{1}{2}\ln\frac{2\Lambda^2}{3\mu^2}=\frac{1}{2}\ln\frac{2}{3}. \tag{B9}$$

The remaining integrals I_1 and I_3 are evaluated similarly. In the process, we need the following sum rules [11,8]:

$$\int_{-q}^{q}\frac{dq_0}{2\pi q_0}\ \beta_l(q_0,q)=\frac{1}{q^2}-\frac{1}{q^2+3\omega_p^2}$$
$$-2\int_q^\infty\frac{dq_0}{q_0}\ \delta[q^2+\Pi_l(q_0/q)],$$

$$\int_{-q}^{q}\frac{dq_0}{2\pi q_0}\ \nu_t(q_0,q)=\frac{1}{q^2+\omega_p^2}-2\int_q^\infty\frac{dq_0}{q_0}\ \delta[q_0^2-q^2$$
$$-\Pi_t(q_0/q)], \tag{B10}$$

where Π_l and Π_t are the polarization functions in the hard thermal loop approximation. (We use the same notations as in Ref. [8].) In the computation of I_3—which involves $\nu_t(q_0,q)$—we change the integration variables as in Eq. (B7) above, and obtain

$$I_3=\frac{1}{2}\ln\frac{3}{2}, \tag{B11}$$

which happens to cancel I_2, Eq. (B9). As for the electric piece I_1, we write

$$I_1=-\int_0^\infty dq\ q\left\{\frac{1}{q^2}-\frac{1}{q^2+3\omega_p^2}\right.$$
$$\left.-2\int_q^\infty\frac{dq_0}{q_0}\ \delta[q^2+\Pi_l(q_0/q)]\right\}$$
$$=\ln\frac{\sqrt{3}\omega_p}{\mu}-2\int_\mu^\infty dq\ q\int_q^\infty\frac{dq_0}{q_0}\ \delta[q^2+\Pi_l(q_0/q)], \tag{B12}$$

where an infrared cutoff μ was introduced when separating the terms inside the braces. In the second term, we change the variables according to

$$x\equiv q_0/q,\quad y\equiv q^2,\quad dq\ dq_0=\frac{1}{2}\ dx\ dy, \tag{B13}$$

and get

$$-\int_1^{x_M}\frac{dx}{x}\int dy\,\delta[y+\Pi_l(x)]=-\ln x_M=-\ln\frac{\omega_p}{\mu}. \tag{B14}$$

The upper limit was obtained as $x_M(\mu)=\omega_l(\mu)/\mu\simeq\mu_p/\mu$ for $\mu\to 0$. From Eqs. (B12) and (B14), we finally obtain

$$I_1=\frac{1}{2}\ln 3, \tag{B15}$$

which is the result quoted in Eq. (3.8).

We finally evaluate the momentum integral in Eq. (3.12) in the nonrelativistic limit $v\ll 1$. Since $|q_0|\leqslant vq\ll q$, we need the spectral functions $\beta_{l,t}(q_0,q)$ only for very small frequencies [18]:

$$\beta_l(q_0\ll q)\simeq\frac{3\pi\omega_p^2(q_0/q)}{(q^2+3\omega_p^2)^2},$$

$$\beta_t(q_0\ll q)\simeq\frac{3\pi\omega_p^2(q_0/2q)}{q^4+(3\pi\omega_p^2q_0/4q)^2}. \tag{B16}$$

Corresponding to the three terms in Eq. (3.12), we write $C(v)=C_1(v)+C_2(v)+C_3(v)$.

The electric contribution is evaluated as

$$C_1(v)=\frac{1}{v^2}\int_0^\infty dq\ q\int_{-vq}^{vq}\frac{dq_0}{2\pi q_0}\ \beta_l(q_0,q)$$
$$\simeq\frac{1}{v^2}\int_0^\infty dq\ q\ \frac{3\omega_p^2v}{(q^2+3\omega_p^2)^2}=\frac{1}{2v}, \tag{B17}$$

where the neglected terms are smaller, at least, by two powers of v [since $\beta_l(q_0,q)$ is an odd function of q_0].

The first magnetic contribution is

$$C_2(v)=-\frac{1}{v^2}\int_0^\infty dq\ q\int_{-vq}^{vq}\frac{dq_0}{2\pi q_0}\frac{q_0^2}{q^2}\ \beta_t(q_0,q)$$
$$\simeq-\frac{8}{3\pi^2\omega_p^2v}\int_0^\infty dq\ q\left[1-\frac{\arctan y(q;v)}{y(q;v)}\right], \tag{B18}$$

where we have used the approximate expression (B16) for $\beta_t(q_0,q)$ to perform the integral over q_0, and we have denoted $y(q;v)\equiv 3\pi\omega_p^2v/(4q^2)$. In the remaining integral over q, we make the obvious change of variables $y(q;v)\equiv t$, with $dq/q=dt/(2t)$, and obtain

$$C_2(v)=\frac{1}{\pi}\int_0^\infty\frac{dt}{t^2}\left[1-\frac{\arctan t}{t}\right]$$
$$=\frac{1}{\pi}\int_0^\infty dy[1-y\ \operatorname{arccoty}]=\frac{1}{4}, \tag{B19}$$

which is independent of v.

Finally, the second magnetic contribution reads

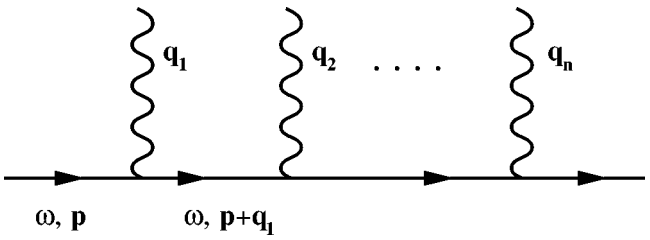

FIG. 5. A typical diagram contributing to $G(x,y|\mathbf{A})$ to order g^n in perturbation theory. This diagram involves n gluon field insertions, and $n+1$ free propagators G_0 (including the external lines). The external fields are purely static and magnetic.

$$C_3(v)=\int_0^\infty dq\ q\int_{-vq}^{vq}\frac{dq_0}{2\pi q_0}\ \nu_t(q_0,q)$$
$$\simeq\int_0^\infty\frac{dq}{q}\left[\frac{2}{\pi}\arctan y(q;v)-\frac{\omega_p^2}{q^2+\omega_p^2}\right],\quad\text{(B20)}$$

where we have also used the definition (3.4) of $\nu_t(q_0,q)$. Note that, for any $v>0$, the remaining integral over q is well defined, and saturated by soft momenta $q\lesssim\omega_p$. Still, the limit $v\to 0$ is not well defined (because of potential infrared singularities), so that we need to perform the momentum integral before studying the small v behavior. By using the same change of variables as above, we rewrite Eq. (B20) as

$$C_3(v)\simeq\int_0^\infty\frac{dt}{2t}\left[\frac{2}{\pi}\arctan t-\frac{t}{t+\tilde{v}}\right]$$
$$=\int_0^1 dt\ \frac{\arctan t}{\pi t}+\int_1^\infty\frac{dt}{\pi t}\left[\arctan t-\frac{\pi}{2}\right]+\frac{1}{2}\ln\tilde{v},\quad\text{(B21)}$$

with $\tilde{v}\equiv 3\pi v/4$. The two integrals in the second line mutually cancel, as can be seen by changing $t\to 1/t$ in any of them, and then using $\arctan 1/t=\pi/2-\arctan t$. Finally,

$$C_3(v)\simeq\frac{1}{2}\ln\tilde{v}.\quad\text{(B22)}$$

By putting together the above results in Eqs. (B17), (B19), and (B22), one obtains the result quoted in Eq. (3.13).

APPENDIX C

In Sec. V above, we have used a non-Abelian version of the Bloch-Nordsieck model to study the interactions between hard quasiparticles (quarks or gluons) and soft virtual gluons in hot QCD. In this appendix, we examine the validity of this approximation for the case where the hard quasiparticle is a transverse gluon.

The dominant contributions to the hard ($p\gtrsim T$) gluon propagator near the mass shell at $\omega=p$ (i.e., the leading infrared divergences for $\omega\to p$) come from the diagrams illustrated in Fig. 4. The continuous line there represents the hard gluon and the wavy lines denote very soft ($q\ll gT$) static ($q_0=0$) magnetic gluons. Once again, our strategy is to consider first the interactions with a classical, static, color field $\mathbf{A}^a(q)$. Then, a typical diagram looks as in Fig. 5. The self-energy corrections in Fig. 4 will be eventually recovered by functional integration, as shown in Eq. (5.10).

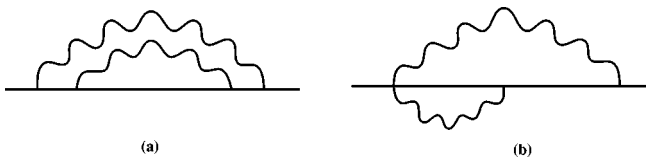

FIG. 6. Some two-loop self-energy corrections in QCD. The continuous line represents a hard gluon, which is nearly on shell. The wavy lines are soft magnetostatic gluons. In the on-shell limit, diagram (b), which also involves a four-gluon vertex, is less infrared singular than diagram (a).

A noteworthy feature of Figs. 5 and 4 is that the hard particle is involved only in three-gluon (but not in four-gluon) vertices. [Of course, the four-gluon vertices do also enter the self-energy diagrams—see, e.g., Fig. 4—but they couple only soft internal gluons; cf. Eq. (5.10).] The reason is that, to a given order in perturbation theory, the diagrams which involve the hard particle in four-gluon vertices are less infrared singular. This can be easily verified by power counting: Consider, e.g., the two two-loop graphs in Fig. 6. For $\omega=p$, the diagram in Fig. 6(a), with only three-gluon vertices, gives rise to a linear infrared singularity. That is, its contribution to the damping rate is of the order $\gamma^{(2a)}\sim g^4T^2/\mu$ (up to logarithms of gT/μ), which for $\mu\sim g^2T$ gives $\gamma^{(2a)}\sim g^2T$; i.e., it is of the same order as the one-loop contribution. (This leading divergence can be isolated by using the simplified BN Feynman rules to be derived below. See Appendix C in Ref. [8] for a detailed analysis.) The diagram in Fig. 6(b), which also involves one four-gluon vertex, may give rise, at most, to logarithmic mass-shell singularities. We thus expect $\gamma^{(2b)}\sim g^4T^2/p\sim g^4T$, which stands beyond our present accuracy, and should be discarded for consistency. We shall verify shortly that, for the problem at hand, neglecting the four-gluon vertices is indeed consistent with gauge symmetry.

Consider the diagram in Fig. 5, with only three-gluon vertices. The latter are linear in the external gluon momenta:

$$-igf^{abc}\Gamma_{ijl}(\mathbf{p},\mathbf{q},\mathbf{k})=-igf^{abc}[(p-q)_l\delta_{ij}+(q-k)_i\delta_{jl}$$
$$+(k-p)_j\delta_{il}],\quad\text{(C1)}$$

where $\mathbf{p}+\mathbf{q}+\mathbf{k}=0$. Remember that all the external lines in Fig. 5 are of the magnetic type, so that we need just the spacial components of the vertex function. Furthermore, color indices play no special role for the subsequent kinematic approximations, and will be omitted in intermediate formulas.

For all the vertices in Fig. 5, one of the external momenta is soft, since it is carried by the classical color field. If q is the soft momentum in Eq. (C1), then

$$\Gamma_{ijl}(\mathbf{p},\mathbf{q},\mathbf{k})\simeq\Gamma_{ijl}(\mathbf{p},0,-\mathbf{p})=p_l\delta_{ij}+p_i\delta_{jl}-2p_j\delta_{il}\,.\quad\text{(C2)}$$

Since the approximate three-gluon vertex (C2) is independent of the soft momentum $\mathbf{q}$, the Ward identities are consistent with setting the four-gluon vertex to zero, which is what we did before.

Consider now a typical internal gluon line in Fig. 5: It is necessarily hard and nearly on shell. In the Coulomb gauge, the associated propagator reads (recall that $q_0=0$)

$$D_{ij}(\omega,\mathbf{p}+\mathbf{q})=\frac{\delta_{ij}-(\hat{p}_i+\hat{q}_i)(\hat{p}_j+\hat{q}_j)}{\omega^2-(\mathbf{p}+\mathbf{q})^2}\simeq\frac{1}{2p}\,\frac{\delta_{ij}-v_iv_j}{\omega-\mathbf{v}\cdot(\mathbf{p}+\mathbf{q})}, \tag{C3}$$

where $\hat{p}_i=p_i/p\equiv v_i$ and the approximate equality holds since $q\ll p$ and $\omega\sim p$. That is, $D_{ij}(\omega,\mathbf{p}+\mathbf{q})\simeq(1/2p)\mathcal{P}_{ij}G_0(\omega,\mathbf{p}+\mathbf{q})$, where $\mathcal{P}_{ij}=\delta_{ij}-v_iv_j$ is a transverse projector, and G_0 is the BN propagator [cf. Eq. (1.1)]:

$$G_0(\omega,\mathbf{p}+\mathbf{q})=\frac{1}{\omega-\mathbf{v}\cdot(\mathbf{p}+\mathbf{q})}. \tag{C4}$$

In Fig. 5, all the three-gluon vertices such as Eq. (C2) appear between projectors such as $\mathcal{P}_{ij}$. By using the identity

$$\mathcal{P}_{im}\Gamma_{mjn}(\mathbf{p},0,-\mathbf{p})\mathcal{P}_{nl}=-2(\delta_{il}-v_iv_l)p_j=-2p\mathcal{P}_{il}v_j, \tag{C5}$$

it can then be easily verified that the leading contribution of the diagram 5 to the hard gluon propagator can be evaluated with the following simplified Feynman rules (we reintroduce here the color indices): (i) the hard particle propagator $\delta^{ab}G_0(\omega,\mathbf{p}+\mathbf{q})$, and (ii) the hard particle-soft gluon vertex $igf^{abc}v_i$. These are the Feynman rules which have been used to define the non-Abelian Bloch-Nordsieck model in Sec. VI. For a hard quark, the color indices in the above Feyman rules should be replaced by the corresponding indices in the fundamental representation.

[1] F. Bloch and A. Nordsieck, Phys. Rev. **52**, 54 (1937).

[2] N. N. Bogoliubov and D. V. Shirkov, *Introduction to the Theory of Quantized Fields* (Interscience, New York, 1959).

[3] H. A. Weldon, Phys. Rev. D **44**, 3955 (1991); **49**, 1579 (1994).

[4] E. Braaten and R. D. Pisarski, Nucl. Phys. **B337**, 569 (1990); Phys. Rev. D **42**, R2156 (1990); J. Frenkel and J. C. Taylor, Nucl. Phys. **B334**, 199 (1990); J. C. Taylor and S. M. H. Wong, *ibid.* **B346**, 115 (1990); R. Efraty and V. P. Nair, Phys. Rev. D **47**, 5601 (1993); R. Jackiw and V. P. Nair, *ibid.* **48**, 4991 (1993).

[5] J. P. Blaizot and E. Iancu, Nucl. Phys. **B417**, 608 (1994); **B434**, 662 (1995).

[6] J. P. Blaizot, J.-Y. Ollitrault, and E. Iancu, in *Quark-Gluon Plasma 2*, edited by R. C. Hwa (World Scientific, Singapore, 1996).

[7] J. P. Blaizot and E. Iancu, Phys. Rev. Lett. **76**, 3080 (1996).

[8] J. P. Blaizot and E. Iancu, Phys. Rev. D **55**, 973 (1997).

[9] R. D. Pisarski, Phys. Rev. Lett. **63**, 1129 (1989).

[10] V. V. Lebedev and A. V. Smilga, Ann. Phys. (N.Y.) **202**, 229 (1990); Phys. Lett. B **253**, 231 (1991).

[11] R. D. Pisarski, Phys. Rev. D **47**, 5589 (1993).

[12] T. Altherr, E. Petitgirard, and T. del Rio Gaztelurrutia, Phys. Rev. D **47**, 703 (1993); H. Heiselberg and C. J. Pethick, *ibid.* **47**, R769 (1993); S. Peigné, E. Pilon, and D. Schiff, Z. Phys. C **60**, 455 (1993); A. V. Smilga, Phys. At. Nucl. **57**, 519 (1994); R. Baier and R. Kobes, Phys. Rev. D **50**, 5944 (1994); A. Niégawa, Phys. Rev. Lett. **73**, 2023 (1994); F. Flechsig, H. Schulz, and A. K. Rebhan, Phys. Rev. D **52**, 2994 (1995).

[13] S. Weinberg, *The Quantum Theory of Fields I* (Cambridge University Press, Cambridge, England, 1995).

[14] E. Braaten, Phys. Rev. Lett. **74**, 2164 (1995).

[15] K. Farakos, K. Kajantie, K. Rummukainen, and M. Shaposhnikov, Nucl. Phys. **B425**, 67 (1994); K. Kajantie, M. Laine, K. Rummukainen, and M. Shaposhnikov, *ibid.* **B458**, 90 (1996).

[16] M. Le Bellac, *Thermal Field Theories* (Cambridge University Press, Cambridge, England, 1996).

[17] V. V. Klimov, Sov. Phys. JETP **55**, 199 (1982); H. A. Weldon, Phys. Rev. D **26**, 1394 (1982).

[18] R. D. Pisarski, Physica A **158**, 146 (1989).

[19] W. Magnus, F. Oberhettinger, and R. P. Soni, *Formulas and Theorems for the Special Functions of Mathematical Physics* (Springer-Verlag, Berlin, 1966).

[20] R. Baier, G. Kunstatter, and D. Schiff, Phys. Rev. D **45**, 4381 (1992); Nucl. Phys. **B388**, 287 (1992).

[21] A. K. Rebhan, Phys. Rev. D **46**, 4779 (1992).

[22] D. Sen, Phys. Rev. D **41**, 1227 (1990).

[23] J. P. Blaizot and E. Iancu, Nucl. Phys. **B459**, 559 (1996).

[24] A. Linde, Phys. Lett. **96B**, 289 (1980); D. J. Gross, R. D. Pisarski, and L. G. Yaffe, Rev. Mod. Phys. **53**, 43 (1981).

[25] E. Fradkin, Proc. Lebedev Phys. Inst. **29**, 7 (1965); J. P. Blaizot, E. Iancu, and R. Parwani, Phys. Rev. D **52**, 2543 (1995).

[26] B. Vanderheyden and J. Y. Ollitrault, Phys. Rev. D **56**, 5108 (1997).